

TOPOLOGY OPTIMIZATION IN FLUID DYNAMICS USING ADJOINT-BASED TRUNCATED NEWTON

Dimitrios I. Papadimitriou, Evangelos M. Papoutsis-Kiachagias and Kyriakos C.
Giannakoglou

National Technical University of Athens,
School of Mechanical Engineering,
Lab. Of Thermal Turbomachines,
Parallel CFD & Optimization Unit
Zografou, Athens, 15710, Greece

e-mails: dpapadim@mail.ntua.gr, vaggelisp@gmail.com, kgianna@central.ntua.gr

Keywords: Continuous adjoint approach, topology optimization, second-order sensitivities, Truncated Newton, loss minimization, duct flows.

Abstract. *This paper proposes a truncated Newton algorithm for efficiently solving topology optimization problems in fluid mechanics, such as the design of ducts with optimal performance. In topology optimization problems, where the number of design variables i.e. the porosity function values at each grid cell (in cell-centered methods) or node (vertex-centered), are too many, the adjoint approach is, by far, the most efficient way to compute the gradient required by any descent algorithm, since the CPU cost per gradient computation is independent of the number of the design variables. Although the Newton method requires only a few cycles to locate the optimal solution, the computation of the exact Hessian matrix is prohibitively expensive since its cost scales with the number of design variables. The proposed truncated Newton solves the Newton equation iteratively, without computing the exact Hessian matrix itself. Instead, Hessian-vector products are efficiently computed using second-order sensitivity analysis based on the adjoint approach and direct differentiation. Just a few conjugate gradient iterations for the solution of the Newton equations are enough to satisfactorily accelerate the convergence rate of the objective function value. Thus far, the truncated Newton was applied to shape optimization problems according to geometrical parameterization schemes which define the design variables. It is the first time such an algorithm is presented for the solution of topology optimization problems. The method is applied to the topology optimization of ducted laminar flows, by minimizing the total pressure losses between the given inlet and outlet boundaries of the flow domain.*

1 INTRODUCTION

Topology optimization is quite a new area of interest in fluid dynamics. In structure mechanics, the first relevant paper dates back to 1988, [1], where the scope was to optimize structures for maximum stiffness, by controlling the material layout within a predefined space. For this purpose, a local (i.e. at each grid node or cell, depending on the formulation) criterion that defines whether this should be treated as solid or not was used. In structural mechanics, other applications of topology optimization can be found in [2] and [3] for structures with high deformations. Topology optimization methods have also been developed for acoustic problems, [4], and the design of micromechanisms, [5].

In CFD-based optimization, the first topology optimization methods were developed for creeping flows, where viscous effects dominate [6, 7]. Setting up a topology optimization method in fluid mechanics requires some of the flow equations to be replaced by

$$CFE + \alpha \cdot CSS = 0 \quad (1)$$

over the computational domain. In eq. 1, CFE denotes the flow equations in their conventional form (i.e. those to be satisfied at any point within the flow domain, according to the selected flow model), α is the so-called porosity field and CSS stands for the conditions at the surrounding solid part of the domain. Topology optimization aims at computing the optimal field of α which minimizes an objective function F , such as the viscous losses between the pre-specified inlet(s) to and outlet(s) from the flow domain to be determined. Other objective functions could be used instead; for instance, a topology optimization problem might aim at designing a flow channel that maximizes the heat exchange between the flowing fluid and the surrounding solid, etc. From the practical point of view, particularly when manifolds with more than one exits must be designed, the problem is usually constrained, since the optimal solution must also fulfill other requirements, such as a desirable mass flow rate per exit, etc. Based on the above formulation, the topology optimization problem has as many unknowns (design variables, i.e. porosity α values) as the number of grid nodes (in vertex-centered schemes) or that of grid cells (in cell-centered schemes). As such, all gradient-based solution methods, must be supported by tools for computing the gradient of F at a cost that doesn't scale with the number of design variables; this is why, the adjoint method used in this paper is the perfect choice. Upon completion of the optimization problem, the computed α values determine the shape of the sought flow channel. Areas with zero α (practically, $\alpha \leq \epsilon$; ϵ is an infinitesimal positive quantity) correspond to parts of the domain where fluid flows since, there $CFE = 0$. In contrast, areas with non-zero α (practically, $\alpha \geq \epsilon$) correspond to the surrounding solid since, there, $CSS = 0$. The interface between the two distinct areas is the boundary (line in $2D$ or surface in $3D$) of the channel to be designed. In contrast to structural mechanics, the literature of topology optimization in fluid mechanics is not that rich. In [8], the laminar Navier-Stokes equations were used as the flow model. In [9], topology optimization for turbulent flows is demonstrated, by making, however, the frozen turbulence assumption. In the same paper, the adjoint approach is used to compute the gradient of the total pressure losses function with respect to the porosity control variables.

Since its first appearance in [10], the adjoint approach has been efficiently used for the shape design and optimization of various configurations, [11, 12, 13], by providing the gradient of the objective function with respect to the design parameters at a cost independent of the number of these parameters, to efficiently drive a gradient-based optimization method towards the optimal solution. Extensions of the adjoint approach to the computation of second-order sensitivity derivatives, for use in the Newton method, can also be found, [14, 15]. In these studies, a

method for the computation of the exact Hessian matrix was proposed and its use within the Newton optimization algorithm accelerated the convergence of F to its minimum. However, since the cost for computing the Hessian matrix still scales with the number of design variables, its use is restricted to problems with reasonably few of them. Should the problem size increases, an efficient alternative is the exactly initialized quasi-Newton method, where the exact Hessian matrix is computed only at the first cycle and, then, is approximately updated as in standard quasi-Newton methods; however, in the case of topology optimization with so many design variables, the exact Hessian matrix cannot be computed even once.

Alternatively, the Newton system of equations may be solved iteratively (truncation of the Newton equations, [16, 17]) requiring only the computation of Hessian-vector products instead of the complete Hessian matrix. This algorithm applied to shape optimization problems was presented by the authors in [18]. This method proved to perform well in cases with a relatively high number of design variables (an order of 50 design variables was used). The truncated Newton based on the continuous adjoint approach and direct differentiation has also been presented in variational data assimilation problems in meteorology, [19, 20, 21, 22] and, along with Automatic Differentiation techniques, in [23].

In this paper, the truncated Newton method is applied to topology optimization of laminar flows. The design variables are many more than those used in shape optimization problems. Two applications are shown concerning the design of 2D ducts. The first one, including 38400 design variables (or grid cells) in total, has one inlet and one outlet with a squared blockage in the center and the second one contains 73600 design variables and has two inlets, two outlets and three squared blockages. The truncated Newton algorithm is found to accelerate the convergence rate, minimizing the objective function value faster and to a lower value than a conventional gradient-based algorithm.

2 PROBLEM FORMULATION AND OPTIMIZATION METHOD

Let us assume that a flow channel, connecting inlet S_I and outlet S_O boundaries which are specified by the designer, must be designed, so as to give a flow with minimum total pressure losses. The flow is considered to be laminar and the fluid is incompressible. This is a typical optimization problem in internal aerodynamics, associated with an objective function expressing the mass-averaged total pressure losses, by

$$F = - \int_{S_I} \left(p + \frac{1}{2} v^2 \right) v_i n_i dS - \int_{S_O} \left(p + \frac{1}{2} v^2 \right) v_i n_i dS \quad (2)$$

Starting point for the formulation of the topology optimization problem, apart from the objective function of eq. 2, is the system of flow equations which define the so-called state or primal problem. After artificially introducing the porosity field α into the conventional flow equations for the laminar flow of an incompressible fluid, these become, [9],

$$\begin{aligned} R^p &= \frac{\partial v_j}{\partial x_j} = 0 \\ R_i^v &= v_j \frac{\partial v_i}{\partial x_j} + \frac{\partial p}{\partial x_i} - \frac{\partial}{\partial x_j} \left[\nu \left(\frac{\partial v_i}{\partial x_j} + \frac{\partial v_j}{\partial x_i} \right) \right] + \alpha v_i = 0, \quad i = 1, 2 \end{aligned} \quad (3)$$

Based on the notation of eq. 1, the last terms in the momentum equations are those previously abbreviated to CSS in eq. 1. In areas where $\alpha \geq \epsilon$, eqs. 3 are satisfied only if $v_i = 0$ and these define the solid surrounding of the channel, see also [9]. In eqs. 3, p is the static pressure

divided by the density and ν the kinematic viscosity. Dirichlet boundary conditions are imposed for the inlet velocities and the outlet pressure whereas zero Neumann conditions for the velocity at the outlet and the pressure at the inlet.

In the present study, the solution of the state problem is performed using the OpenFOAM[®] software, [24], which is a toolbox equipped with a high-level symbolic application programming interface. OpenFOAM employs a cell-centered storage for the flow variables; in topology optimization, the porosity values α are also stored at the N grid cell centers.

The minimization of F , eq. 2, subject to eqs. 3, can be performed via steepest descent, quasi-Newton or (exact) Newton methods. The use of the adjoint method in either of them is practically the only affordable way to compute the derivatives of F , for reasons explained in the introduction. This paper sticks with the use of Newton methods which will be employed without, however, computing the exact Hessian of F . The Newton method is based on

$$\frac{\delta^2 F}{\delta \alpha_m \delta \alpha_n} \delta \alpha_n = - \frac{\delta F}{\delta \alpha_m}, \quad \alpha_n|^{k+1} = \alpha_n|^{k} + \delta \alpha_n|^{k} \quad (4)$$

where k is the optimization cycle counter.

As mentioned in the introduction, the most efficient way of computing the Hessian matrix $\frac{\delta^2 F}{\delta \alpha_m \delta \alpha_n}$, has a computational cost that scales with the number of design variables N . Theoretically, it is straightforward to extend the methods presented in [14, 15] to topology optimization and conclude that the most efficient way to compute the Hessian of F is by employing the Direct Differentiation (DD) method for $\frac{\delta F}{\delta \alpha_m}$, followed by the Adjoint Variable (AV) method for the $\frac{\delta^2 F}{\delta \alpha_m \delta \alpha_n}$. The DD approach requires the solution of PDEs similar to eqs. 3, for the derivatives of the flow variables with respect to the porosity. N systems of the DD equations must be solved; the cost for solving each one of them is practically equal to the cost of solving the state problem, i.e. the flow equations. Throughout this paper, this cost will be denoted by EFS (“Equivalent Flow Solution”). Therefore, in contrast to shape optimization problems which, comparatively, have a reasonable number of design variables, the DD-AV approach cannot be used to solve problems with excessively high N values, such as topology optimization problems.

To the authors’ knowledge, this paper presents, for the first time in the literature, the implementation of the truncated Newton method for the solution of topology optimization problems. Following a previous work by the authors, [18], dealing with the use of truncated Newton in shape optimization, the purpose of the present paper is to extend the same technique to topology optimization and assess its performance with comparisons to other possible solution techniques.

Here, the truncated Newton method is based on the use of the Conjugate Gradient (CG) method with M_{CG} cycles for the solution of linear systems, where M_{CG} should be relatively small to keep the computational cost at low levels.

The CG-based truncated Newton method for optimization problems was inspired by the way the CG method solves any linear system, such as $A_{mn}x_n = q_m$, $(m, n) \in [1, N]$. Starting from the initialization $x^\rho = x^0$ and the corresponding residuals $r^\rho = r^0 = A_{mn}x_n^0 - q_m^0$ and $s_m^0 = -r_m^0$,

the following steps,

$$\begin{aligned}
w_m &= A_{nm}s_n, \quad m \in [1, N] \\
\eta &= \frac{r_m^\rho r_m^\rho}{s_m w_m} \\
x_m^{\rho+1} &= x_m^\rho + \eta s_m, \quad m \in [1, N] \\
r_m^{\rho+1} &= r_m^\rho + \eta w_m, \quad m \in [1, N] \\
\beta &= \frac{r_m^{\rho+1} r_m^{\rho+1}}{r_m^\rho r_m^\rho} \\
s_m &= -r_m^{\rho+1} + \beta s_m, \quad m \in [1, N]
\end{aligned} \tag{5}$$

must be performed iteratively ($\rho \leftarrow \rho + 1$; ρ is the CG cycle counter) as long as the norm of the new residual $r^{\rho+1}$ exceeds a user-defined threshold value. The cost of each CG cycle, comprising the previous six steps, is approximately equal to the cost of performing the matrix-vector multiplication of the first step. Based on the previous stopping criterion, the CG method is expected to terminate after M_{CG} cycles, where $M_{CG} \leq N$.

In optimization problems, the Newton equation, eq. 4, looks similar to the aforementioned linear system example, if $A_{mn} = \frac{\delta^2 F}{\delta \alpha_m \delta \alpha_n}$ and $q_m = -\frac{\delta F}{\delta \alpha_m}$. The non-linearity of eq. 4, due to the non-linear state equations, requires the CG iterative algorithm to be performed within the optimization loop (counter $k = 1, \dots, k_{max}$). As already mentioned, the number of CG cycles (M_{CG}) (inner loop within each optimization cycle) is a small, user-defined integer. In each optimization cycle, four main steps must be executed: (a) solve the flow equations, anew (b) compute $\frac{\delta F}{\delta \alpha_m}$ (c) compute the Hessian-vector products $\frac{\delta^2 F}{\delta \alpha_m \delta \alpha_n} \alpha_n$ and, finally, (d) solve eq. 4 iteratively by employing M_{CG} cycles of the CG algorithm. The computation of the first-order gradient is conducted using the continuous adjoint approach. Hessian-vector products are computed using the AV-DD method. The latter means that the (continuous) adjoint variable (AV) method is used to compute the gradient, followed by the direct differentiation (DD) of the flow and adjoint equations to compute the Hessian-vector products (see section 3).

3 THE CONTINUOUS AV METHOD IN TOPOLOGY OPTIMIZATION

The computation of the first-order sensitivity derivatives using the continuous AV method is based on a formulation presented in [9] for the functional of eq. 2. The augmented objective function F_{aug} is introduced

$$F_{aug} = F + \int_{\Omega} u_i R_i^v d\Omega + \int_{\Omega} q R^p d\Omega \tag{6}$$

and its sensitivities with respect to the design variables α_m read

$$\frac{\delta F_{aug}}{\delta \alpha_m} = \frac{\delta F}{\delta \alpha_m} + \int_{\Omega} u_i \frac{\delta R_i^v}{\delta \alpha_m} d\Omega + \int_{\Omega} q \frac{\delta R^p}{\delta \alpha_m} d\Omega \tag{7}$$

where u_i are the adjoint to the velocity components v_i and q is the adjoint pressure. The resulting terms are treated by using the Green–Gauss theorem. For instance, the viscous terms are integrated by parts, as follows

$$\begin{aligned}
-\int_{\Omega} \nu u_i \frac{\partial}{\partial x_j} \left[\frac{\partial}{\partial x_j} \left(\frac{\delta v_i}{\delta \alpha_m} \right) \right] d\Omega &= -\int_S \nu u_i \frac{\partial}{\partial x_j} \left(\frac{\delta v_i}{\delta \alpha_m} \right) n_j dS + \int_S \nu \frac{\partial u_i}{\partial x_j} \frac{\delta v_i}{\delta \alpha_m} n_j dS \\
&\quad - \int_{\Omega} \nu \frac{\partial^2 u_i}{\partial x_j^2} \frac{\delta v_i}{\delta \alpha_m} d\Omega
\end{aligned} \tag{8}$$

$$\begin{aligned}
 - \int_{\Omega} \nu u_i \frac{\partial}{\partial x_j} \left[\frac{\partial}{\partial x_i} \left(\frac{\delta v_j}{\delta \alpha_m} \right) \right] d\Omega &= - \int_S \nu u_i \frac{\partial}{\partial x_i} \left(\frac{\delta v_j}{\delta \alpha_m} \right) n_j dS + \int_S \nu \frac{\partial u_i}{\partial x_j} \frac{\delta v_j}{\delta \alpha_m} n_i dS \\
 &\quad - \int_{\Omega} \nu \frac{\partial^2 u_i}{\partial x_i \partial x_j} \frac{\delta v_j}{\delta \alpha_m} d\Omega
 \end{aligned} \tag{9}$$

where $S = S_I \cup S_O \cup S_W$, S_W being the initial solid walls of the domain Ω (i.e. its contour, excluding S_I and S_O) where the topology optimization problem is solved.

Using eqs. 8 and 9 and treating the remaining terms in a similar way, eq. 7 gives

$$\begin{aligned}
 \frac{\delta F_{aug}}{\delta \alpha_m} &= \frac{\delta F}{\delta \alpha_m} + \int_S \left[u_j v_j n_i + u_i v_j n_j + \nu \left(\frac{\partial u_i}{\partial x_j} + \frac{\partial u_j}{\partial x_i} \right) n_j - q n_i \right] \frac{\delta v_i}{\delta \alpha_m} dS \\
 &\quad - \int_S \nu \frac{\delta}{\delta \alpha_m} \left(\frac{\partial v_i}{\partial x_j} + \frac{\partial v_j}{\partial x_i} \right) n_j u_i dS \\
 &\quad + \int_S \left\{ -v_j \left(\frac{\partial u_j}{\partial x_i} + \frac{\partial u_i}{\partial x_j} \right) - \nu \frac{\partial}{\partial x_j} \left(\frac{\partial u_i}{\partial x_j} + \frac{\partial u_j}{\partial x_i} \right) + \frac{\partial q}{\partial x_i} + \alpha u_i \right\} \frac{\delta v_i}{\delta \alpha_m} d\Omega \\
 &\quad + \int_S u_j n_j \frac{\delta p}{\delta \alpha_m} dS - \int_{\Omega} \frac{\partial u_j}{\partial x_j} \frac{\delta p}{\delta \alpha_m} d\Omega + \int_{\Omega} u_i v_i \frac{\delta \alpha}{\delta \alpha_m} d\Omega
 \end{aligned} \tag{10}$$

By eliminating field integrals containing the variations in the flow variables, the field adjoint equations

$$\begin{aligned}
 R^q &= \frac{\partial u_j}{\partial x_j} = 0 \\
 R_i^u &= -v_j \left(\frac{\partial u_i}{\partial x_j} + \frac{\partial u_j}{\partial x_i} \right) - \nu \frac{\partial}{\partial x_j} \left(\frac{\partial u_i}{\partial x_j} + \frac{\partial u_j}{\partial x_i} \right) + \frac{\partial q}{\partial x_i} + \alpha u_i = 0, \quad i = 1, 2
 \end{aligned} \tag{11}$$

are derived. All boundary integrals must be processed in a similar way. It can be shown that (a) along S_I , the normal primal and adjoint velocities must be equal and the tangential adjoint velocities must be zeroed, i.e.

$$u_{\langle n \rangle} = v_{\langle n \rangle}, \quad u_{\langle t \rangle} = 0$$

(b) along S_O , the following two conditions must be satisfied,

$$q = u_j v_j + u_{\langle n \rangle} v_{\langle n \rangle} + \nu \left(\frac{\partial u_i}{\partial x_j} + \frac{\partial u_j}{\partial x_i} \right) n_j n_i - \frac{3}{2} v_{\langle n \rangle}^2 - \frac{1}{2} v_{\langle t \rangle}^2 \tag{12a}$$

$$0 = u_{\langle t \rangle} v_{\langle n \rangle} + \nu \left(\frac{\partial u_i}{\partial x_j} + \frac{\partial u_j}{\partial x_i} \right) n_j t_i - v_{\langle n \rangle} v_{\langle t \rangle} \tag{12b}$$

and (c) along S_W , the conditions

$$u_{\langle n \rangle} = 0, \quad u_{\langle t \rangle} = 0$$

should be met. Once the adjoint PDEs and their boundary conditions are satisfied, the sensitivity derivatives result from eq. 10, as follows

$$\frac{\delta F}{\delta \alpha_m} = \int_{\Omega} u_i v_i \frac{\delta \alpha}{\delta \alpha_m} d\Omega = u_i^m v_i^m \Omega^m \tag{13}$$

where m indicates the cell index. The above analysis is restricted to laminar flows. For shape optimization problems, the authors have already presented the exact continuous adjoint approach to the Spalart-Allmaras turbulence model, [25]. It seems straightforward to extend this to the truncated Newton method, but this is beyond the scope of this paper. In such a case, a very “careful” treatment at the regions close to the wall is required.

Working with steepest descent, the values of α could be updated by

$$\alpha_n|^{k+1} = \alpha_n|^{k} - \eta \left. \frac{\delta F}{\delta \alpha_n} \right|^{k} \quad (14)$$

where η is a user-defined small positive scalar value and k the optimization cycle counter. The steepest descent approach will be used as reference, for comparing the convergence of the truncated Newton algorithm with.

4 COMPUTATION OF HESSIAN-VECTOR PRODUCTS

Once the gradient of F is computed through eq. 13 using the AV method, its expression is differentiated (DD) to yield $\frac{\delta^2 F}{\delta \alpha_m \delta \alpha_n}$ and, then, multiplied with s_n so as to give the Hessian-vector products appearing in the CG algorithm (eq. 5, for $A_{mn} = \frac{\delta^2 F}{\delta \alpha_m \delta \alpha_n}$)

$$\begin{aligned} \frac{\delta^2 F}{\delta \alpha_m \delta \alpha_n} s_n &= \int_{\Omega} \left(v_i \frac{\delta u_i}{\delta \alpha_n} s_n + u_i \frac{\delta v_i}{\delta \alpha_n} s_n \right) \frac{\delta \alpha}{\delta \alpha_m} d\Omega = \int_{\Omega} (\bar{u}_i v_i + u_i \bar{v}_i) \frac{\delta \alpha}{\delta \alpha_m} d\Omega \\ &= (\bar{u}_i^m v_i^m + u_i^m \bar{v}_i^m) \Omega^m \end{aligned} \quad (15)$$

where $\frac{\delta v_i}{\delta \alpha_n} s_n = \bar{v}_i$ and $\frac{\delta u_i}{\delta \alpha_n} s_n = \bar{u}_i$ are new fields to be computed. To this end, the flow and adjoint equations (eqs. 3 and 11, respectively) are differentiated w.r.t. α and, then, multiplied with s yielding two new systems of PDEs, which can be solved for \bar{v}_i and \bar{u}_i . The first system is

$$\begin{aligned} \frac{\partial \bar{v}_j}{\partial x_j} &= 0 \\ \bar{v}_j \frac{\partial v_i}{\partial x_j} + v_j \frac{\partial \bar{v}_i}{\partial x_j} + \frac{\partial \bar{p}}{\partial x_i} - \frac{\partial}{\partial x_j} \left[\nu \left(\frac{\partial \bar{v}_i}{\partial x_j} + \frac{\partial \bar{v}_j}{\partial x_i} \right) \right] + \alpha \bar{v}_i + s v_i &= 0, \quad i = 1, 2 \end{aligned} \quad (16)$$

whereas the second

$$\begin{aligned} \frac{\partial \bar{u}_j}{\partial x_j} &= 0 \\ -\bar{v}_j \left(\frac{\partial u_i}{\partial x_j} + \frac{\partial u_j}{\partial x_i} \right) - v_j \left(\frac{\partial \bar{u}_i}{\partial x_j} + \frac{\partial \bar{u}_j}{\partial x_i} \right) - \nu \frac{\partial}{\partial x_j} \\ \left(\frac{\partial \bar{u}_i}{\partial x_j} + \frac{\partial \bar{u}_j}{\partial x_i} \right) + \frac{\partial \bar{q}}{\partial x_i} + \alpha \bar{u}_i + s u_i &= 0, \quad i = 1, 2 \end{aligned} \quad (17)$$

The boundary conditions for systems 16 and 17 are derived from the differentiation of the flow and adjoint boundary conditions w.r.t. α_m and the multiplication with s_m . At the inlet,

$$\begin{aligned} \bar{v}_{\langle n \rangle} &= \bar{u}_{\langle n \rangle} = 0 \\ \bar{v}_{\langle t \rangle} &= \bar{u}_{\langle t \rangle} = 0 \\ \frac{\partial \bar{p}}{\partial x_j} n_j &= \frac{\partial \bar{q}}{\partial x_j} n_j = 0 \end{aligned} \quad (18)$$

at the outlet,

$$\bar{p} = 0 \quad (19a)$$

$$\frac{\partial \bar{v}_i}{\partial x_j} n_j = 0 \quad (19b)$$

$$\begin{aligned} \bar{q} = & u_j \bar{v}_j + \bar{u}_j v_j + u_{\langle n \rangle} \bar{v}_{\langle n \rangle} + \bar{u}_{\langle n \rangle} v_{\langle n \rangle} + \nu \left(\frac{\partial \bar{u}_i}{\partial x_j} + \frac{\partial \bar{u}_j}{\partial x_i} \right) n_j n_i \\ & - 3v_{\langle n \rangle} \bar{v}_{\langle n \rangle} - v_{\langle t \rangle} \bar{v}_{\langle t \rangle} \end{aligned} \quad (19c)$$

$$0 = u_{\langle t \rangle} \bar{v}_{\langle n \rangle} + \bar{u}_{\langle t \rangle} v_{\langle n \rangle} + \nu \left(\frac{\partial \bar{u}_i}{\partial x_j} + \frac{\partial \bar{u}_j}{\partial x_i} \right) n_j t_i - \bar{v}_{\langle n \rangle} v_{\langle t \rangle} - v_{\langle n \rangle} \bar{v}_{\langle t \rangle} \quad (19d)$$

and along the solid walls

$$\begin{aligned} \bar{v}_i = \bar{u}_i = & 0 \\ \frac{\partial \bar{p}}{\partial x_j} n_j = & \frac{\partial \bar{q}}{\partial x_j} n_j = 0 \end{aligned} \quad (20)$$

The cost for solving systems 16 and 17 is almost equal to that of solving twice the flow equations, i.e. equal to 2 EFS. Thus, the overall cost of each optimization cycle for the truncated Newton algorithm based on the segregated handling of the governing equations, is equal to $(2+2M_{CG})$ EFS. This cost comprises one solution of eqs. 3, one of eqs. 11 and M_{CG} solutions of eqs. 16 and 17.

Particularly for topology optimization problems, numerical experiments have shown that it is much faster to solve the optimization problem equations (eqs. 3, 11, 16 and 17) in a ‘‘one shot’’ or ‘‘all-at-once’’ manner, i.e. by performing one iteration of the iterative scheme (such as Jacobi, Gauss Siedel, etc.) per system of equations, and then update the α values using eq. 4 or 14. This can be attributed to the fact that the flow fields change drastically from one optimization cycle to another (so there is no reason to let the state equations converge) and is facilitated by the fact that, in topology optimization, there is no mesh change or deformation. Keeping this in mind, the cost of the optimization algorithms presented in the next section will be measured in linear solver iterations (LSI) instead of EFS, with the cost ratio being as discussed above (2 LSI per steepest descent iteration and $2 + 2M_{CG}$ LSI per truncated Newton iteration).

5 CASE STUDIES

The proposed adjoint-based truncated Newton method for topology optimization is demonstrated in two cases. The first case is concerned with a square design domain with area equal to 1×1 length units including one inlet and one outlet boundary with lengths equal to $0.2 m$ each, and a square body (‘‘obstacle’’) at the middle of the domain. A computational grid of 38400 cells is used, which implies that there are 38400 design variables or unknown α values. The velocity profile at the inlet is parabolic with its maximum value equal to $0.28 m/s$.

The second case also uses the same square domain as Ω and has two inlet and two outlet boundaries with length equal to $0.2 m$ each and three square bodies inside. The computational grid consists of 73600 cells.

The distributions of the optimal primal and adjoint velocity magnitudes for the first case, computed using the truncated Newton approach, are shown in fig. 1. The same fields computed using steepest descent are shown in fig. 2. The optimal porosity distributions using the two approaches is presented in fig. 3. Slight differences can be observed after close inspection.

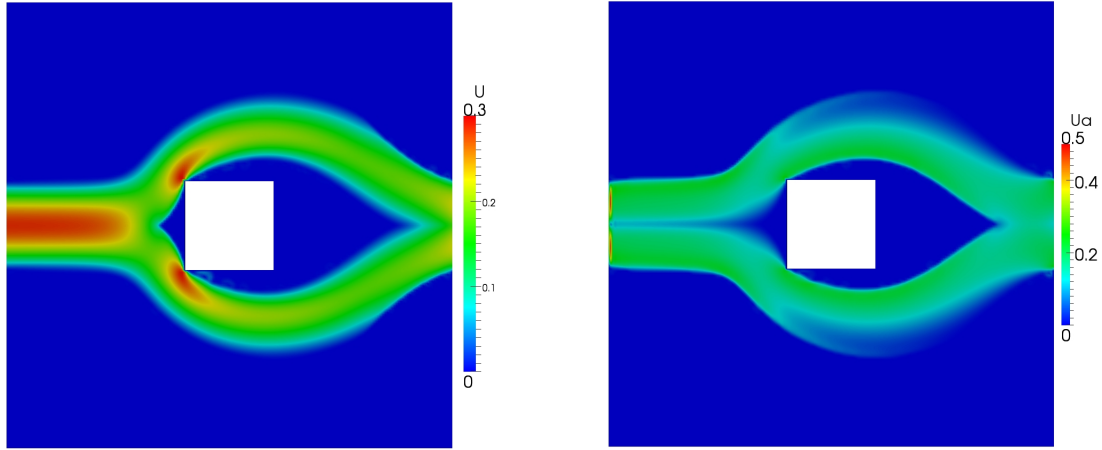


Figure 1: Topology optimization of a duct with a single obstacle. Distributions of the optimal primal and (top-left), adjoint velocity (top-right) magnitudes, computed using the truncated Newton approach.

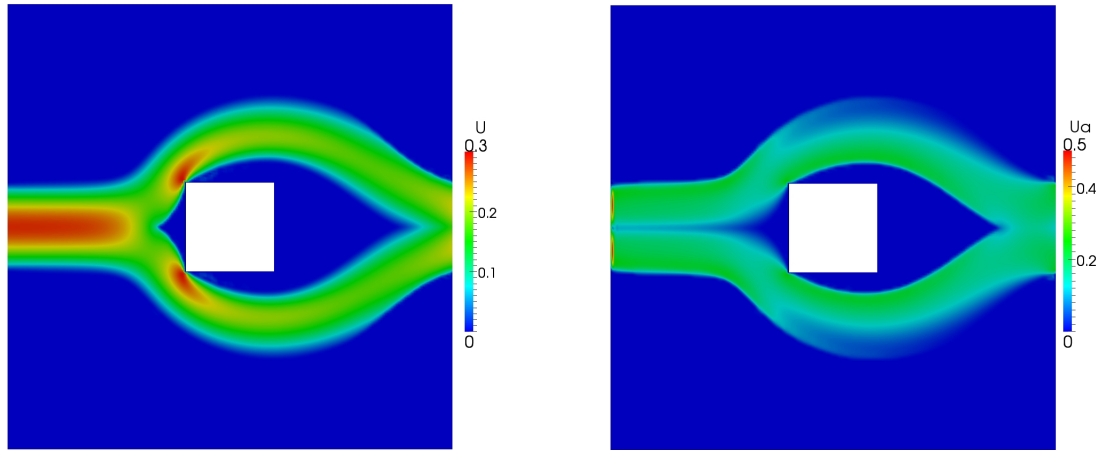


Figure 2: Topology optimization of a duct with a single obstacle. Distributions of the optimal primal and (left), adjoint velocity (right) magnitudes, computed using steepest descent.

However, as shown below, the convergence rates and the optimal value of the objective function differ.

The convergence rates of steepest descent and truncated Newton for the first case are shown in fig. 4, in terms of CPU cost (LSI). All the equations are solved in a one-shot manner.

In fig. 4 (top) the red solid line corresponds to the convergence of the steepest descent algorithm and the other lines correspond to the convergence of the truncated Newton algorithm, initialized from different phases of the steepest descent one. The use of steepest descent at the first optimization phase offers a good initialization for the truncated Newton method. It can be seen that the cycle at which the truncated Newton starts, does not affect much the optimized result. Thus, it is recommended to start the truncated Newton cycles after the steepest descent has only partially converged, overcoming the first “rough” one-shot cycles, at which the truncated Newton might face numerical difficulties.

In fig. 4 (top) a parametric study of the number of conjugate gradient sub-iterations is shown. The four curves marked with TN, correspond to $M_{CG} = 5$, $M_{CG} = 10$, $M_{CG} = 20$ and $M_{CG} = 40$. It can be deduced that, for the problem at hand, the lower M_{CG} value gives the best convergence of the truncated Newton algorithm, since higher M_{CG} values increase the cost per optimization cycle without proportionally accelerating the convergence.

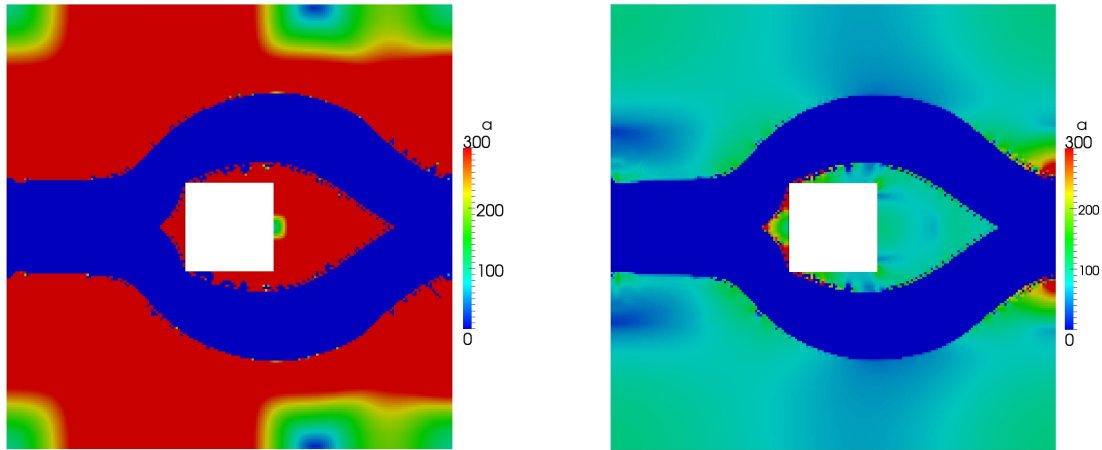


Figure 3: Topology optimization of a duct with a single obstacle. Distributions of the optimal porosity variable computed using the truncated Newton approach (left) and steepest descent (right).

For the second case, the optimal velocity distributions using steepest descent and truncated Newton are shown in fig. 5. Although the figures are much alike, there are slight differences that allow the objective function value to converge 4% lower when using the truncated Newton algorithm instead of the steepest descent one, fig. 6. This can be related to the fact that in a problem with more than 70000 variables, steepest descent can be easily trapped to a local minimum, whereas the second-order truncated Newton method has a greater possibility to overcome it.

6 CONCLUSIONS

The truncated Newton algorithm with conjugate gradient sub-iterations was applied for the first time in the literature to the topology optimization of duct flows. The number of design variables was equal to the number of grid cells, which was 73600 in the largest case examined. Using so many design variables would have made the cost of computing the exact Hessian prohibitive. Instead, the truncated Newton algorithm, utilizing the (continuous) AV-DD method to compute Hessian-vector products instead of the exact Hessian, proved to accelerate the convergence to the optimal topology, when compared to the steepest descent algorithm, which was, however, an essential ingredient of the process, since it was used to initialize it. The CPU cost has decreased in both cases examined and the objective function value converged deeper when compared to a pure steepest descent approach, by avoiding entrapment to local minima.

ACKNOWLEDGEMENTS

The study was supported by the Basic Research Program “PEVE 2010” of the National Technical University of Athens.

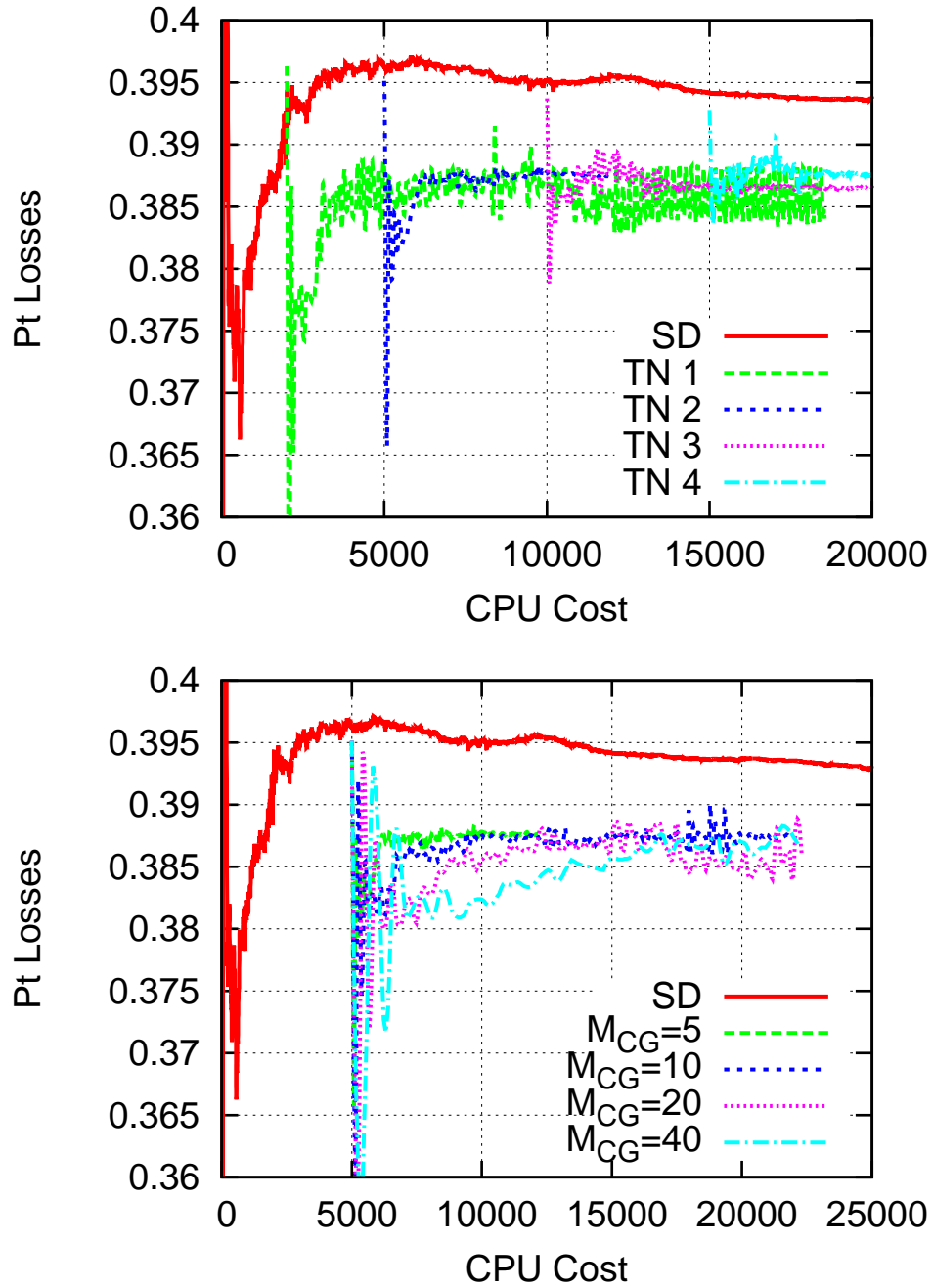


Figure 4: Topology optimization of a duct with a single obstacle. Convergence of pt losses ($\frac{F}{\frac{1}{2}v_{in}^2 m_{in}}$, where m_{in} is the inlet volume flow rate and v_{in} is the inlet velocity magnitude) using the truncated Newton algorithm, initialized after different steepest descent steps (top) and using different number of conjugate gradient sub-iterations (bottom).

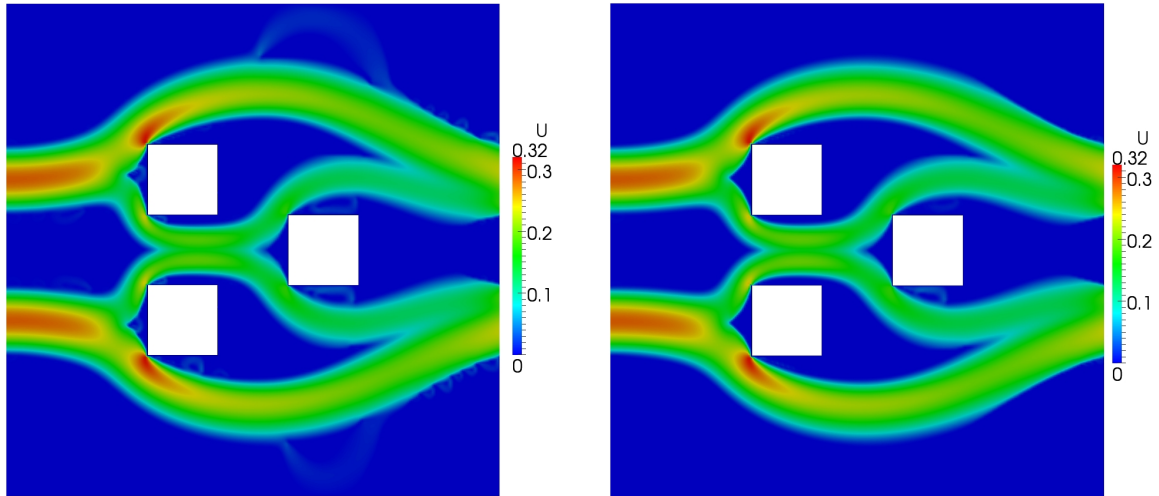


Figure 5: Topology optimization of a duct with three obstacles. Optimal primal velocity distributions computed using the truncated Newton approach (left) and steepest descent (right).

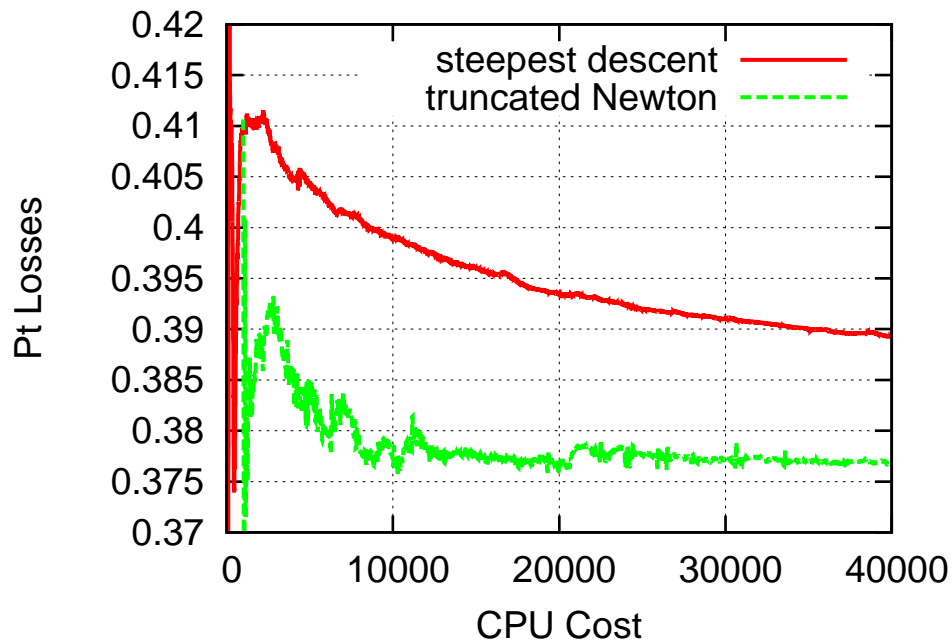


Figure 6: Topology optimization of a duct with three obstacles. Convergence of pt losses ($\frac{F}{\frac{1}{2}v_{in}^2 m_{in}}$, where m_{in} is the inlet volume flow rate and v_{in} is the inlet velocity magnitude) using the truncated Newton algorithm, starting after the application of steepest descent for 1000 cycles.

REFERENCES

- [1] Bendsoe M., Kikuchi N.: Generating optimal topologies in structural design using a homogenization method, *Computer Methods in Applied Mechanical Engineering*, 71 (1988), 197–224.
- [2] Bendsoe M. Sigmund O.: *Topology Optimization - Theory, Methods and Applications*, Springer Verlag, 2004.
- [3] Buhl T., Pedersen C.B.W., Sigmund O.: Stiffness design of geometrically non-linear structures using topology optimization, *Structural and Multidisciplinary Optimization*, 19 (2000), 93-104.
- [4] Jensen J.: Photonic band gaps and vibrations in 1D and 2D mass-spring structures, *Journal of Sound & Vibration*, 266 (2003), 1053–1078.
- [5] Larsen U., Sigmund O.: Design and fabrication of compliant micromechanisms and structures with negative Poisson's ratio, *IEEE Journal of Microelectromechanical Systems*, 1997.
- [6] Borrvall T., Petersson J.: Topology optimization of fluids in Stokes flow, *International Journal for Numerical Methods in Fluids*, 41 (2003), 77-107.
- [7] Guest J., Prvost J.: Topology optimization of creeping fluid flows using a Darcy-Stokes finite element, *International Journal for Numerical Methods in Engineering*, 66 (2006), 461-484.
- [8] Gersborg-Hansen A., Sigmund O., Haber R.B.: Topology optimization of channel flow problems, *Structural and Multidisciplinary Optimization*, 30 (2005), 181–192.
- [9] Othmer C.: A continuous adjoint formulation for the computation of topological and surface sensitivities of ducted flows, *International Journal for Numerical Methods in Fluids*, 58(2008), 861-877.
- [10] Pironneau O: On optimum design in fluid mechanics. *Journal of Fluid Mechanics*, 64 (1974), 97–110.
- [11] Jameson A: Aerodynamic design via control theory. *Journal of Scientific Computing*, 3 (1988), 233–260.
- [12] Anderson WK, Venkatakrishnan V: Aerodynamic design optimization on unstructured grids with a continuous adjoint formulation. *AIAA Paper*, 97-0643, 1997.
- [13] Papadimitriou DI, Giannakoglou KC: A continuous adjoint method with objective function derivatives based on boundary integrals for inviscid and viscous flows. *Journal of Computers & Fluids*, 363 (2007), 25–341.
- [14] Papadimitriou DI., Giannakoglou KC: Aerodynamic shape optimization using first and second order adjoint and direct approaches, *Archives of Computational Methods in Engineering, (State of the Art Reviews)*, 15 (2008), 447-488.

- [15] Zervogiannis T., Papadimitriou DI, Giannakoglou KC; Total Pressure Losses Minimization in Turbomachinery Cascades using the Exact Hessian, *Journal of Computer Methods in Applied Mechanics and Engineering*, 199 (2010), 2697-2708.
- [16] Nocedal J, Wright SJ.: Numerical Optimization, Springer, 1999.
- [17] Nash SG.: A survey of truncated-Newton methods. *Journal of Computational and Applied Mathematics*, 124 (2000), 45–59.
- [18] Papadimitriou DI, Giannakoglou KC.: Aerodynamic Design using the Truncated Newton Algorithm and the Continuous Adjoint Approach, *International Journal for Numerical Methods in Fluids*, 68 (2012), 724–739.
- [19] Wang Z, Navon IM, Zou X, Le Dimet FX.: A truncated Newton optimization algorithm in meteorology applications with analytic Hessian/vector products. *Computational Optimization and Applications*, 4 (1995), 241–262.
- [20] Wang Z, Droegemeier K.: The adjoint Newton algorithm for large-scale unconstrained optimization in meteorology applications. *Computational Optimization and Applications*, 10 (1998), 283–320.
- [21] Le Dimet FX, Navon IM, Daescu DN.: Second-order information in data assimilation. *Monthly Weather Review*, 130 (2002), 629–648.
- [22] Daescu DN, Navon IM.: Efficiency of a POD-based reduced second-order adjoint model in 4D-Var data assimilation. *International Journal for Numerical Methods in Fluids*, 53 (2007), 985–1004.
- [23] Naumann U, Maier M, Riehme J, Christianson B. Automatic first- and second-order adjoints for truncated Newton. *Proceedings of the International Multiconference on Computer Science and Information Technology*, 541-555, 2007.
- [24] <http://www.openfoam.com>
- [25] Zymaris AS, Papadimitriou DI, Giannakoglou KC, Othmer C.: Continuous Adjoint Approach to the Spalart Allmaras Turbulence Model, for Incompressible Flows *Computers & Fluids*, 38 (2009), 1528–1538.